C Journal of Carbon Research

MDPI

Article

Thermal Transport Study in a Strained Carbon Nanotube and Graphene Junction Using Phonon Wavepacket Analysis

Jungkyu Park

Mechanical Engineering, Kennesaw State University, Marietta, GA 30062, USA; jpark186@kennesaw.edu; Tel.: +1-470-578-6809

Abstract: This study investigates single-mode phonon scattering from a junction structure consisting of a (6,6) single-walled carbon nanotube (SWCNT) and graphene, subject to mechanical deformation, using phonon wavepacket analysis. Results show that longitudinal acoustic (LA) and transverse acoustic (TA) phonons at low frequencies are transmitted more effectively through the SWCNT–graphene junction when the junction is deformed. As low-frequency phonons in LA and TA modes are major energy carriers, it is expected that thermal transport across the SWCNT–graphene junction will be more efficient when the junction is deformed. Interfacial thermal resistance across the SWCNT-graphene junction was calculated using reverse nonequilibrium molecular dynamics (RNEMD). The RNEMD results show that the interfacial thermal resistance decreases when the structure is elongated, deforming the junction between the SWCNT and graphene. However, there was no notable difference in the transmission of twisting (TW) and flexural (FO) phonons when the junction was deformed. The study also showed that the transmission of phonon energy through the SWCNT–graphene junction has a slight dependence on the group velocity of phonons, with phonons having higher group velocities transmitting the junction more effectively. The findings of this research will play a significant role in advancing the development of futuristic electronics by providing a tool for developing 3D carbon nanostructures with high thermal performance under mechanical deformation.

Keywords: phonon scattering; carbon nanotube; graphene; deformation

Citation: Park, J. Thermal Transport Study in a Strained Carbon Nanotube and Graphene Junction Using Phonon Wavepacket Analysis. *C* **2023**, *9*, 21. https://doi.org/10.3390/c9010021

Academic Editor: Cédric Pardanaud

Received: 10 December 2022
Revised: 8 February 2023
Accepted: 9 February 2023
Published: 11 February 2023

1. Introduction

The fast-paced advancement in flexible electronics requires the development of lightweight and conductive materials [1,2]. Carbon-based nanomaterials, such as graphene and carbon nanotubes (CNTs) are promising candidates due to their exceptional mechanical and thermal performance [3–8], as well as porous structure. However, their strong directional transport properties limit their application in futuristic electronics. Specifically, single-walled carbon nanotubes (SWCNTs) and graphene possess remarkable in-plane thermal conductivities, but exhibit weak out-of-plane thermal conductivities [9–17].

Three-dimensional carbon nanostructures that consist of CNTs and graphene are expected to transform the outstanding unidirectional transport properties of CNTs and graphene into multi-directional properties [17,18]. The potential applications of 3D carbon nanostructures are numerous and captivating. Due to their light weight and exceptional strength, these structures are ideal for use as a body material in military vehicles, thereby increasing the vehicles' fuel efficiency. Their exceptional thermal conductivity makes them suitable for use in brake systems, enhancing the lifespan of the brakes. Furthermore, their high surface charge density and electrical conductivity make them well-suited for energy-storage devices [19]. Researchers [20–28] showed that 3D carbon nanostructures can improve the efficiency of a Li-ion battery. The multi-directional conductivity and reduced resistance at junctions in 3D carbon nanostructures will enhance the diffusion of lithium ions toward the electrode [29,30]. Their high mechanical strength will provide additional advantages, and their efficient thermal transport property will quickly dissipate heat generated at the anode.

The suitability of 3D carbon nanostructures for flexible electronics is based on their consistent transport properties under mechanical stress. Extensive studies have investigated the impact of mechanical strain on thermal transport in nanostructured materials. [31–33]. Generally, the mechanical strain decreases the thermal conductivity of nanostructured materials. Lee et al. [34] reported ~50% thermal conductivity reduction with a 0.25% strain in aluminum nanofilm. The thermal conductivities of graphene and CNTs are also significantly decreased by strain [35,36]. However, the behavior of transport in 3D carbon nanostructures may differ from that of their constituent nanomaterials, CNTs and graphene, during mechanical deformation. The interconnecting graphene sheets between CNT-graphene junctions in 3D carbon nanostructures can permit stretching without breaking or compromising the C-C bonds in these junctions. This can preserve their thermal transport performance when subjected to mechanical stress.

In this research, we aim to investigate the single-mode phonon scattering in a (6,6) SWCNT and graphene junction structure that is undergoing mechanical deformation. The fraction of transmitted energy of major phonon modes in the SWCNT will be estimated using phonon wavepacket analysis. Furthermore, we will determine the interfacial thermal resistance of the (6,6) SWCNT–graphene junction while undergoing mechanical strain through the application of reverse nonequilibrium molecular dynamics.

2. Simulation Methods

In this study, we utilize phonon wavepacket analysis [37–41], which is a type of molecular dynamics (MD) simulation that involves pre-designed atom coordinates and velocities. This analysis allows us to investigate the phonon transport mechanism by simulating the propagation of a localized vibrational motion of atoms (i.e., wavepacket) until it collides with a SWCNT–graphene junction. The initial atom coordinates and velocities are selected based on a chosen phonon mode with a wavenumber from the phonon dispersion spectra of a SWCNT. We first obtain the phonon dispersion relations by assuming wavelike solutions for the classical equations of motion of atoms.

$$\omega^2(\mathbf{k})\varepsilon_{j\alpha}(\mathbf{k}) = \sum_{j',l',\beta} \frac{1}{\sqrt{m_j m_{j'}}} \Phi_{jl\alpha,j'l'\beta} \exp(i\mathbf{k}\cdot[\mathbf{r}^{j',l'} - \mathbf{r}^{j,l}])\varepsilon_{j'\beta}(\mathbf{k}) \quad (1)$$

Here, $\omega(k)$ is the vibrational frequency which is a function of wave vector k. $\varepsilon_{j\alpha}(k)$ is the eigenvector for the corresponding wave vector. $r_{j,l}$ is the position vector for jth atom in the lth unit cell. For a monatomic crystalline structure with a unidirectional wave vector such as SWCNT, the dynamical matrix is expressed as

$$D_{j\alpha,j'\beta}(k_z) = \frac{1}{m}\sum_{l'} \Phi_{jl\alpha,j'l'\beta} \exp(ik_z[r_z^{j',l'} - r_z^{j,l}]) \quad (2)$$

The force constant $\Phi_{jl\alpha,j'l'\beta}$ is obtained by measuring the α direction force on the jth atom in the lth unit cell when the j'th atom in the l'th unit cell is displaced into β direction by a small distance (small enough not to cause any anharmonicity). To obtain force constants with better accuracy, the crystalline structure is well-equilibrated and energy-minimized at 0 K. Force constants are measured to build the dynamical matrix after displacing basis atoms one by one in the selected reference unit cell into x, y, z directions. Then, eigenvalues and eigenvectors are induced from the constructed dynamical matrix. Using the information in the calculated phonon dispersion relations, initial displacements and velocities of atoms are determined to form a wavepacket. For a monatomic crystalline structure such as SWCNT, the α direction displacement of the jth atom in the lth unit cell is expressed as

$$u_{jl\alpha}(t) = \frac{1}{\sqrt{M}}\sum_{q,\lambda} \varepsilon_{j\alpha}^{\lambda}(k) \exp\left[ik\cdot r_l - iw^{\lambda}(k)t\right] Q(k,\lambda), \quad (3)$$

where λ is phonon mode, k is the wave vector, M is the atomic mass of a carbon atom, ε is the eigenvector, r is the atom position vector, t is time, and $Q(k, \lambda)$ is the amplitude for the corresponding phonon mode and wave vector. The normal modes are summed only for wavenumbers since we want to displace atoms such that they vibrate with a single vibration mode, λ. Therefore, Equation (3) becomes

$$u_{jl\alpha}^{\lambda}(t) = \frac{1}{\sqrt{M}} \sum_{k} \varepsilon_{j\alpha}^{\lambda}(k) \exp\left[ik(z_l - z_0) - i\omega^{\lambda}(k)t\right] Q(k). \quad (4)$$

Here, r is substituted with z (the longitudinal direction of a SWCNT) since the wave vectors in a SWCNT have components of z-direction only. z_l denotes the position of the lth unit cell and z_0 denotes the position of the reference unit cell. The amplitude Q is replaced by a normal distribution function with the selected mean wavenumber k_0 and a standard deviation σ.

$$u_{jl\alpha}^{\lambda}(t) = \frac{A}{\sqrt{M}} \sum_{k} \exp\left[-\frac{(k-k_0)^2}{2\sigma^2}\right] \varepsilon_{j\alpha}^{\lambda}(k) \exp\left[ik(z_l - z_0) - i\omega^{\lambda}(k)t\right], \quad (5)$$

Here, A is an amplification factor and σ is the standard deviation. To propagate a wavepacket into the positive z-direction, velocity vectors are imposed according to the chosen vibrational mode and wavenumber as

$$v_{jl\alpha}^{\lambda}(t) = \frac{A}{\sqrt{M}} \sum_{k} -i\omega^{\lambda}(k) \exp\left[-\frac{(k-k_0)^2}{2\sigma^2}\right] \varepsilon_{j\alpha}^{\lambda}(k) \exp\left[ik(z_l - z_0) - i\omega^{\lambda}(k)t\right]. \quad (6)$$

Initial velocity vectors are obtained by setting t = 0 from the above expression.

The atom coordinates and velocities are chosen to match a selected phonon mode with a specific wavenumber from the phonon dispersion spectra of a SWCNT. The junction structure is comprised of two long (6,6) SWCNTs and a single layer of graphene. The choice of (6,6) SWCNT allows for comparison with previous wavepacket analysis studies of carbon nanotube–graphene junctions [37,41]. The length of a (6,6) SWCNT is approximately 360 nm with 1500 unit cells and the interplanar spacing between junctions is 15 nm. The simulation structure was created using a method detailed in the author's prior research [42] and includes a graphene floor with two holes, combined with two SWCNTs to form seamless junctions with a 5–7 defect, one of the most thermodynamically stable defects in low-dimensional carbon materials (Figure 1b). The wavepacket is created in the simulation structure and propagated through NVE integration. The study simulates two different SWCNT–graphene junction structures, one with a deformed junction and one with an undeformed junction (Figure 1b). The deformed junction was created by applying uniaxial tension in the z direction until the distance between the two SWCNT–graphene junctions reaches 3 nm. Wavepackets were created on the left SWCNT and propagated towards the junction, with the amounts of energy reflected and transmitted recorded for different phonon frequencies.

To better understand thermal transport through a SWCNT–graphene with deformed and undeformed junctions, reverse nonequilibrium molecular dynamics (RNEMD) [43] is employed. In RNEMD, heat flux is imposed by switching energies between a cold bath and hot bath (Figure 2b) until a steady state heat current is reached (approximately 2 ns). Then, the temperature drop across the junction is measured. Interfacial thermal resistance across a junction is obtained by dividing the measured temperature drop by the heat flux imposed by RNEMD algorithm. As described in Figure 2b, two identical junctions are created to maintain the symmetry of the simulation structure to be able to apply periodic boundary conditions in z axis. RNEMD is performed multiple times while gradually stretching the simulation structure in z direction (Figure 2c) to investigate the effect of mechanical strain on thermal resistance across a SWCNT–graphene junction. Before every RNEMD simulation, the simulation structure is equilibrated for about 0.5 ns to obtain statistically

sound simulation results (Figure 2a). RNEMD has been used repeatedly to investigate thermal transport in nanostructured materials [44–48]. The same method was used to estimate the thermal conductivity of SWCNT–graphene junction structures with different diameters in the author's previous research [49].

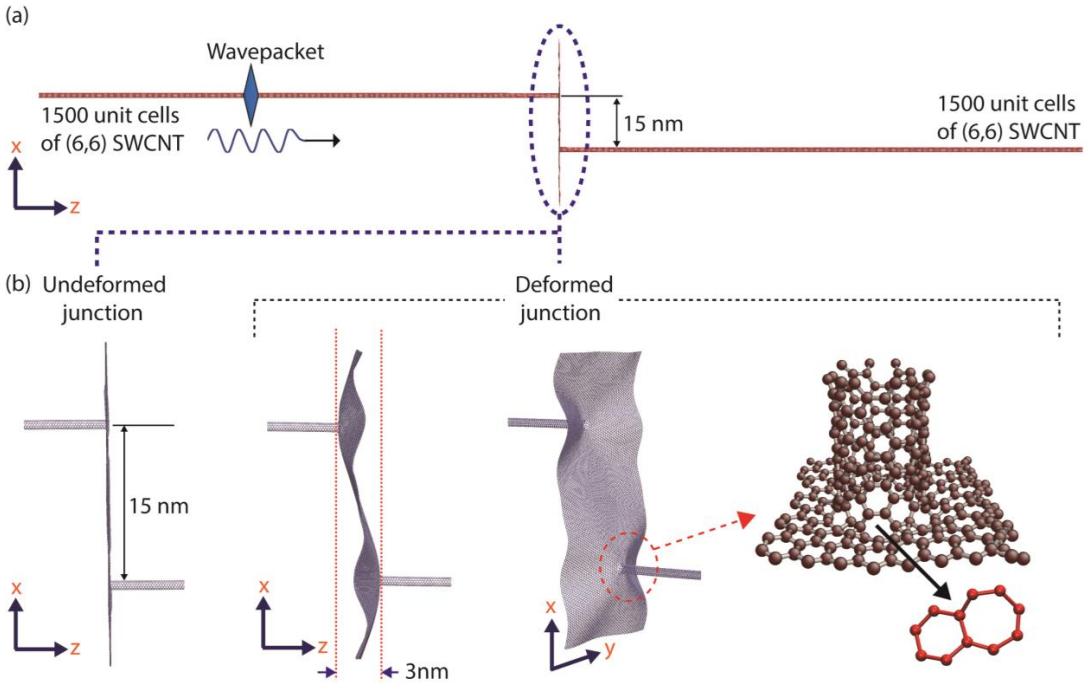

Figure 1. (**a**) The schematic of phonon wavepacket analysis. Interplanar spacing between (6,6) SWCNT–graphene junctions is fixed to be 15 nm. (**b**) Junction structures with undeformed and deformed junctions and a 5–7 defect in the junction are illustrated. The junction structure is deformed uniaxially into *z* direction until the distance between the two SWCNT–graphene junctions reaches 3 nm.

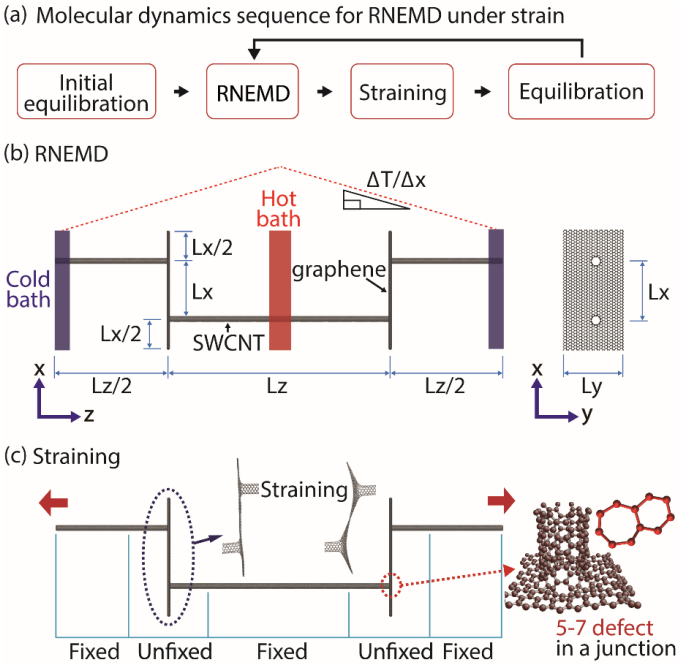

Figure 2. Interfacial thermal resistance estimation for a SWCNT–graphene junction structure under mechanical deformation using RNEMD.

3. Results and Discussions

Figure 3 showcases five significant phonon branches in the selected (6,6) SWCNT. The simulations were carried out using the LAMMPS simulator [50], and the PCFF force field [51] was employed for the phonon wavepacket analysis. The PCFF force field has proven to be a reliable choice in this regard, as its parameters were established from ab initio calculations on microstate at 0 K [52,53], and it has been previously used in numerous phonon wavepacket analyses [37,40,54,55]. The five major phonon modes in carbon nanotubes, Longitudinal Acoustic (LA), Twisting Acoustic (TW), Transverse Acoustic (TA), Radial Breathing (RB), and Flexural Optical (FO), contribute significantly to thermal transport and are depicted in Figure 3b. Among these, the LA mode is the most crucial due to its high group velocity for long-wavelength phonons. RB and FO phonons, being high-group velocity phonons over a broad frequency range, also play a significant role. The total number of phonon branches in a (6,6) SWCNT with 24 basis atoms is 72, of which 42 are visible in Figure 3a as 30 phonon modes are doubly degenerate. Wavepackets were generated on the left SWCNT, as shown in Figure 1, using the phonon dispersion calculation, and allowed to propagate towards the junction.

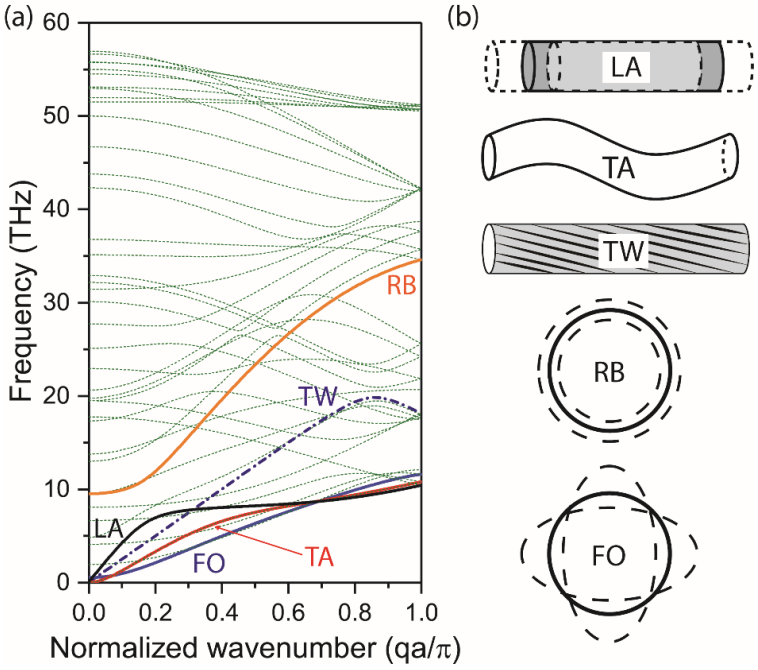

Figure 3. (**a**) Phonon dispersion relations in 1000 unit cells of (6,6) SWCNT. Five important phonon modes, i.e., LA, TA, TW, RB, FO modes are selected in this research. q denotes wave number and a denotes lattice constant. (**b**) Exaggerated illustration of LA, TA, TW, RB, FO vibrational modes.

Figure 4 displays the percentage of energy transmitted by phonons through a SWCNT–graphene junction. As shown in Figure 4a, the percentage of energy transmitted by longitudinal acoustic (LA) phonons is less than 80% and more than 20% of their energies are reflected across the entire frequency range. Park et al. [41] conducted a study on the transmission of phonon energy through a (6,6) SWCNT with point defects. They found that energy transmission in a defective area was generally greater than 90%. As a result, the SWCNT–graphene junction in this study can be considered a significant site of phonon scattering in comparison to point defects. As depicted in Figure 2b, the SWCNT–graphene junction features various defects, such as 5–7, which are likely to scatter incoming phonons, thereby reducing the thermal transport property of 3D carbon nanostructures. The transmission of phonons is somewhat correlated with group velocity for LA, FO, and RB phonons. The energy transmission decreases with a decrease in group velocity. This group velocity dependency of energy transmission has been reported by previous researchers [40,56].

Phonons with high group velocities are more effectively propagated through any irregularities in a crystal structure. However, the dependency of phonon transmission on group velocity in SWCNT–graphene junction structures is not as strong as in SWCNTs with point defects [41]. This is because phonons passing through SWCNT–graphene junctions undergo a complete energy redistribution due to the sudden change in the propagation direction.

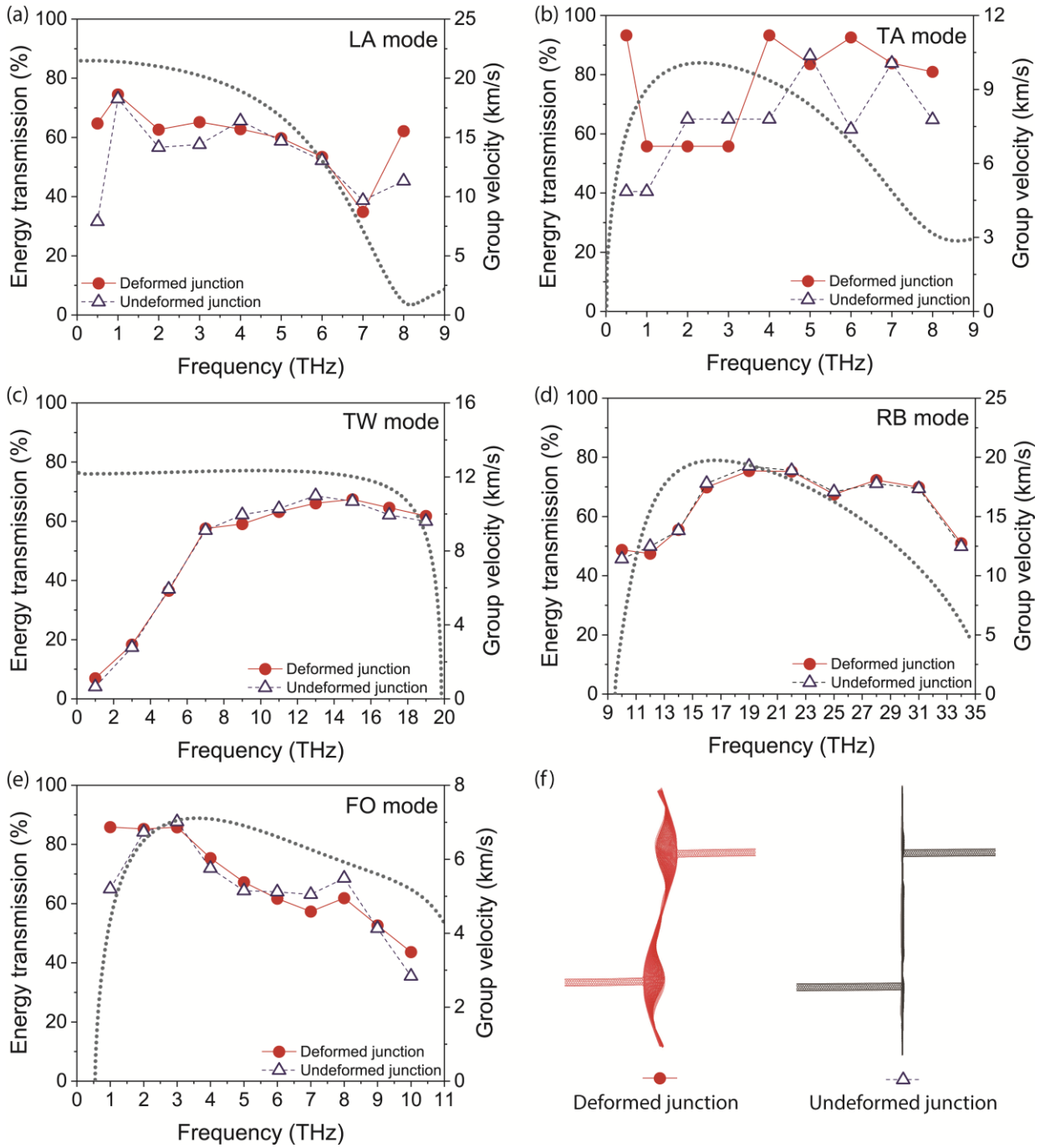

Figure 4. Percent energy transmission through a SWCNT–graphene junction in deformed/undeformed junction structures. Group velocity (dotted dark gray line) is also plotted together. (**a**) LA phonon mode. (**b**) TA phonon mode. (**c**) TW phonon mode. (**d**) RB phonon mode. (**e**) FO phonon mode. (**f**) Illustration of deformed and undeformed junctions.

A significant level of phonon reflection was observed across all phonon frequencies and modes. For instance, with regards to LA phonons, the substantial reflection of low-

frequency phonons (0.5 THz) is likely to significantly impair the thermal transport across the junction. This is because low-frequency LA phonons possess long wavenumbers and high group velocities, as demonstrated in Figure 3. Park et al. [42] reported that interfacial thermal resistance of a (6,6) SWCNT–graphene junction with mixed sp^2/sp^3 bonds and a 50 nm pillar height and 15 nm inter-pillar distance was 3.1×10^{-10} K-m^2/W. The thermal resistance of SWCNT–graphene with pure sp^2 bonds, with a 200 nm pillar height and 5 nm interpillar distance, was reported to be 1.56×10^{-10} K-m^2/W. Phonons passing through a SWCNT–graphene junction must alter their momentum direction to flow over the graphene sheet, which is expected to result in substantial phonon scattering. Additionally, Park et al. [42] calculated the phonon density of states in a SWCNT–graphene junction and found that the frequency and density of populated phonons undergo significant changes when they travel from a SWCNT to a graphene floor. Efficient phonon modes such as LA phonons in a SWCNT must be transformed into significant phonon modes in graphene, such as in-plane phonons, and then reconverted into other significant phonons in a SWCNT. This phonon conversion process is expected to result in a significant amount of energy reflection.

In the instance of TA and TW phonons, unlike LA, RB, and FO phonons, there appears to be no correlation between energy transmission and group velocity. This phenomenon was similarly observed in the case of a SWCNT–SWCNT junction by Park et al. [42]. TA phonons demonstrate the highest level of energy transmission among the five phonons studied, suggesting that TA phonons can be converted to significant phonons in graphene with relative ease in comparison to other phonon modes. Despite low group velocities, RB and FO phonons exhibit strong energy transmission through a junction for low frequencies. Similar results were previously reported in the case of a SWCNT–SWCNT junction [37,42]. However, RB phonons cover a high-frequency regime in the phonon dispersion (Figure 3) and are unlikely to contribute significantly to the thermal transport across the SWCNT–graphene junction.

A noteworthy phenomenon is noted upon a comparison of the energy transmission between an undeformed SWCNT–graphene junction and a deformed SWCNT–graphene junction. The application of mechanical stress results in the deformation of the SWCNT–graphene junction, as depicted in Figure 1b, with the distance between the two SWCNT–graphene interfaces reaching 3 nm. The graphene substrate adjusts smoothly to accommodate this elongation, with no additional defects being produced aside from the pre-existing 5–7 defects. A comparable pattern in energy transmission, expressed as a percentage, is apparent in both the deformed and undeformed junctions. It has been observed that the percent energy transmission in a SWCNT–graphene junction decreases as the group velocity decreases. However, in the case of longitudinal acoustic (LA) phonons (as depicted in Figure 4a), there is a noticeable increase in energy transmission in the lower frequency range (below 4 THz) when the junction is deformed. This suggests that, for LA mode, phonons with high group velocities (low frequencies) are better able to traverse a deformed SWCNT–graphene junction than an undeformed one. This is because, in a deformed junction, phonons do not encounter abrupt changes in the direction of their transport as they reach the graphene floor, which results in more efficient phonon transport compared to an undeformed junction. In the case of TA phonons (as depicted in Figure 4b), the deformed junction demonstrates improved phonon energy transmission across a wide range of frequencies, with the exception of 2 and 3 THz. However, for TW and RB phonons, the deformation of the junction does not significantly impact phonon energy transmission. This suggests that the redistribution of these phonon modes in the graphene floor of the junction structure is not very effective, regardless of any distortions in the crystal structure of the junction. To more effectively investigate this phonon transformation, a wavepacket analysis of junction structures with varying lengths of graphene floor is needed as the permissible phonon wavenumber is limited by the size of the graphene floor.

It is important to note that the present wavepacket analysis was unable to examine the impact of anharmonic effects on energy transmission due to the limited amplitude of the

incident wavepackets, which were kept below 2 picometers to preserve their shape during propagation through the SWCNT–graphene junction.

Another simulation was conducted utilizing molecular dynamics and the reverse nonequilibrium molecular dynamics (RNEMD) method to assess the impact of mechanical strain on the thermal resistance at the interface of both deformed and undeformed SWCNT–graphene junctions. The simulation was conducted using the widely adopted AIREBO force field [57]. This force field has a proven track record of providing valuable insights into the thermal transport properties of carbon-based nanomaterials, as evidenced by previous studies [46,58–60]. The results of the simulation, which depict the interfacial thermal resistance of a SWCNT–graphene junction structure with a 200 nm SWCNT pillar and a 15 nm graphene floor, are displayed as a function of the structure's elongation at temperatures of 10 K, 100 K, and 300 K (as shown in Figure 5).

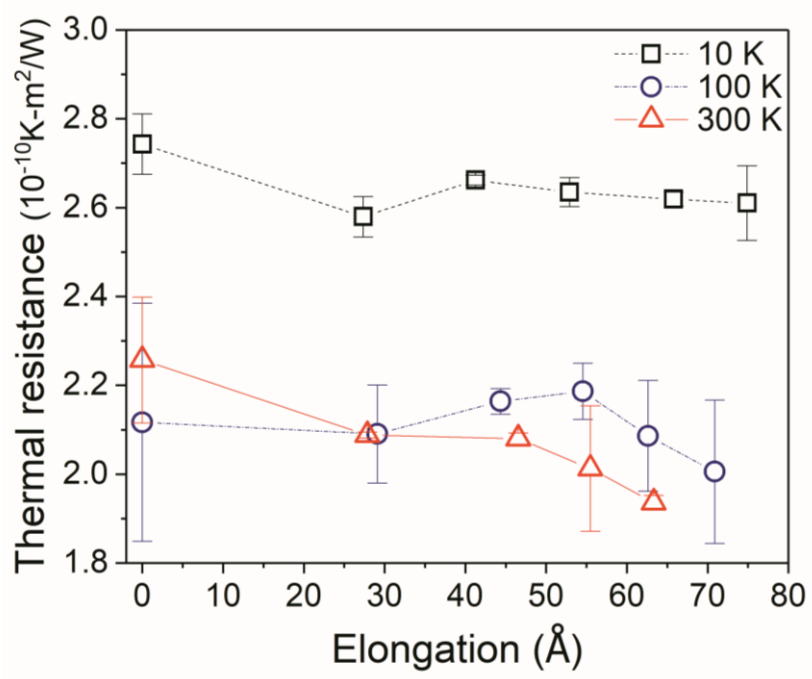

Figure 5. Interfacial thermal resistance as a function of elongation in SWCNT–graphene junction structure at different temperatures. The SWCNT pillar height is 200 nm and the graphene floor size between junctions is 15 nm.

As predicted by the wavepacket analysis, the interfacial thermal resistances are slightly decreased with an increase in elongation. This indicates that the thermal transport through a SWCNT–graphene junction becomes more efficient when the junction is deformed. At low temperatures (10 K), most of the phonons present are long-wavelength phonons. Thus, the decrease in thermal resistance with an increase in mechanical strain at 10 K is attributed to low-frequency phonons, such as LA phonons with frequencies lower than 4 THz and TA phonons with frequencies lower than 2 THz. Park et al. [49] investigated the thermal conductivity of various SWCNT–graphene junction structures and found that thermal conductivity decreases with a decrease in the graphene floor size between junctions. Since the allowable phonon wavelength depends on the size of graphene and SWCNTs, it is expected that the strain effect on the interfacial thermal resistance will be more pronounced when the graphene floor size between junctions and the length of SWCNTs become larger.

It is challenging to link the decrease in thermal resistance across a SWCNT–graphene junction at high temperatures with the results from the wavepacket analysis, as the PCFF potential used in the wavepacket analysis is based on 0 K temperature. Generally, interfacial thermal resistance is lower at high temperatures because thermal transport is already diffusive due to Umklapp scattering at high temperatures, and the amount of scattering

from a SWCNT–graphene junction becomes relatively small compared to low temperatures. At higher temperatures, more high-frequency phonons are expected to be populated, while low-frequency phonons are more prevalent at low temperatures. Thus, it can be assumed that the decrease in thermal resistance from a deformed SWCNT–graphene junction at high temperatures (100 K and 300 K) is due to the higher energy transmission of high-frequency phonons in a deformed junction, as demonstrated in the TA phonon mode (Figure 4b). As demonstrated in other phonon modes (Figure 4a,c–e), energy transmission does not show a significant improvement through mechanical deformation at high frequencies. Thus, the decrease in thermal resistance with an increase in mechanical strain at high temperatures is believed to be due to the fact that phonons do not experience a significant change in their propagation direction when the junction structure is elongated and deformed. It is assumed that SWCNT–graphene junctions erase the memory of the incoming phonon's momentum and redistribute the energy. However, when the junction is deformed, the energy redistribution becomes less drastic as the graphene floor between the junctions is no longer perpendicular to the direction of the SWCNTs. It is important to note that excessive deformation and distortion in the junction structure may ultimately deteriorate the thermal transport performance across the junction, as severe deformation can introduce various defects that negatively impact thermal transport. In this regard, Park et al. [46] simulated the impact of various defects on thermal transport in carbon nanomaterials and found that severely distorted defects, such as divacancies, degrade the thermal conductivity of a carbon nanotube more severely compared to a stable 5–7 defect, which is a major defect in the junction structure simulated in the current study.

4. Conclusions

In the current study, a phonon wavepacket analysis was employed utilizing the PCFF potential to examine the single-mode phonon scattering in both deformed and undeformed SWCNT–graphene junctions. The LA, TA, TW, RB, and FO phonons were selected for the examination. Furthermore, reverse nonequilibrium molecular dynamics simulations were utilized with the AIREBO potential to estimate the interfacial thermal resistance across both the deformed and undeformed junctions.

The results indicate that the transmission of phonon energy is correlated with the group velocity of the phonons. Phonons with higher group velocities demonstrate greater energy transmission through a SWCNT–graphene junction. A deformed SWCNT–graphene junction generally exhibits higher transmission rates for LA and TA phonons for long wavelength phonons. As long wavelength LA and TA phonons are significant heat carriers in carbon nanostructures, it is expected that a deformed junction will transmit heat energy more effectively compared to an undeformed junction, as confirmed by the interfacial thermal resistance calculation results.

At temperatures of 10 K, 100 K, and 300 K, it was found that the interfacial thermal resistance across a SWCNT–graphene junction decreases with an increase in mechanical strain. This is due to the fact that in a deformed junction, phonons do not need to undergo a substantial change in transport direction or undergo complete energy redistribution, while in an undeformed junction, the transport direction must change radically and erase the momentum of incoming phonons. The findings of the present study will be utilized in the design of novel carbon nanomaterials for future flexible electronics and wearable devices.

Funding: This research received no external funding.

Data Availability Statement: The data presented in this study are available on request from the corresponding author.

Acknowledgments: This work was supported in part by research computing resources and technical expertise via a partnership between Kennesaw State University's Office of the Vice President for Research and the Office of the CIO and Vice President for Information Technology.

Conflicts of Interest: The authors declare no conflict of interest.

References

1. Kumar, A.; Zhou, C. The race to replace tin-doped indium oxide: Which material will win? *ACS Nano* **2010**, *4*, 11–14. [CrossRef]
2. Wassei, J.K.; Kaner, R.B. Graphene, a promising transparent conductor. *Mater. Today* **2010**, *13*, 52–59. [CrossRef]
3. Liew, K.; He, X.; Wong, C. On the study of elastic and plastic properties of multi-walled carbon nanotubes under axial tension using molecular dynamics simulation. *Acta Mater.* **2004**, *52*, 2521–2527. [CrossRef]
4. Liew, K.; Wong, C.H.; He, X.; Tan, M.-J.; Meguid, S.A. Nanomechanics of single and multiwalled carbon nanotubes. *Phys. Rev. B* **2004**, *69*, 115429. [CrossRef]
5. Jiang, J.-W.; Wang, J.-S.; Li, B. Young's modulus of graphene: A molecular dynamics study. *Phys. Rev. B* **2009**, *80*, 113405. [CrossRef]
6. Lee, C.; Wei, X.; Kysar, J.W.; Hone, J. Measurement of the elastic properties and intrinsic strength of monolayer graphene. *Science* **2008**, *321*, 385–388. [CrossRef]
7. Zheng, Y.; Wei, N.; Fan, Z.; Xu, L.; Huang, Z. Mechanical properties of grafold: A demonstration of strengthened graphene. *Nanotechnology* **2011**, *22*, 405701. [CrossRef]
8. Balandin, A.; Ghosh, S.; Teweldebrhan, D.; Calizo, I.; Bao, W.; Miao, F.; Lau, C.N. Extremely high thermal conductivity of graphene: Prospects for thermal management applications in silicon nanoelectronics. In Proceedings of the 2008 IEEE Silicon Nanoelectronics Workshop, Honolulu, HI, USA, 15–16 June 2008; pp. 1–2. [CrossRef]
9. Berber, S.; Kwon, Y.K.; Tomanek, D. Unusually high thermal conductivity of carbon nanotubes. *Phys. Rev. Lett.* **2000**, *84*, 4613–4616. [CrossRef] [PubMed]
10. Yu, C.H.; Shi, L.; Yao, Z.; Li, D.Y.; Majumdar, A. Thermal conductance and thermopower of an individual single-wall carbon nanotube. *Nano Lett.* **2005**, *5*, 1842–1846. [CrossRef]
11. Pop, E.; Mann, D.; Wang, Q.; Goodson, K.; Dai, H.J. Thermal conductance of an individual single-wall carbon nanotube above room temperature. *Nano Lett.* **2006**, *6*, 96–100. [CrossRef]
12. Che, J.W.; Cagin, T.; Goddard, W.A. Thermal Conductivity of Carbon Nanotubes. *Nanotechnology* **2000**, *11*, 65–69. [CrossRef]
13. Balandin, A.; Ghosh, S.; Bao, W.; Calizo, I.; Teweldebrhan, D.; Miao, F.; Lau, C.N. Superior thermal conductivity of single-layer graphene. *Nanoletters* **2008**, *8*, 902–907. [CrossRef] [PubMed]
14. Hu, J.; Ruan, X.; Chen, Y.P. Thermal conductivity and thermal rectification in graphene nanoribbons: A molecular dynamics study. *Nano Lett.* **2009**, *9*, 2730–2735. [CrossRef]
15. Cai, W.; Moore, A.L.; Zhu, Y.; Li, X.; Chen, S.; Shi, L.; Ruoff, R.S. Thermal transport in suspended and supported monolayer graphene grown by chemical vapor deposition. *Nano Lett.* **2010**, *10*, 1645–1651. [CrossRef] [PubMed]
16. Sun, K.; Stroscio, M.A.; Dutta, M. Thermal conductivity of carbon nanotubes. *J. Appl. Phys.* **2009**, *105*, 074316. [CrossRef]
17. Park, J.; Prakash, V. Thermal resistance across interfaces comprising dimensionally mismatched carbon nanotube-graphene junctions in 3D carbon nanomaterials. *J. Nanomater.* **2014**, *2014*, 4. [CrossRef]
18. Varshney, V.; Patnaik, S.S.; Roy, A.K.; Froudakis, G.; Farmer, B.L. Modeling of thermal transport in pillared-graphene architectures. *ACS Nano* **2010**, *4*, 1153–1161. [CrossRef] [PubMed]
19. Dimitrakakis, G.K.; Tylianakis, E.; Froudakis, G.E. Pillared graphene: A new 3-D network nanostructure for enhanced hydrogen storage. *Nano Lett.* **2008**, *8*, 3166–3170. [CrossRef]
20. Lee, S.-H.; Sridhar, V.; Jung, J.-H.; Karthikeyan, K.; Lee, Y.-S.; Mukherjee, R.; Koratkar, N.; Oh, I.-K. Graphene–nanotube–iron hierarchical nanostructure as lithium ion battery anode. *ACS Nano* **2013**, *7*, 4242–4251. [CrossRef]
21. Kang, C.; Baskaran, R.; Hwang, J.; Ku, B.-C.; Choi, W. Large scale patternable 3-dimensional carbon nanotube–graphene structure for flexible Li-ion battery. *Carbon* **2014**, *68*, 493–500. [CrossRef]
22. Das, S.; Li, J.; Hui, R. Impact of Electrode Surface/Volume Ratio on Li-ion Battery Performance. In Proceedings of the COMSOL Conference, Boston, MA, USA; 2014; pp. 8–10.
23. Bae, S.-H.; Karthikeyan, K.; Lee, Y.-S.; Oh, I.-K. Microwave self-assembly of 3D graphene-carbon nanotube-nickel nanostructure for high capacity anode material in lithium ion battery. *Carbon* **2013**, *64*, 527–536. [CrossRef]
24. Wang, W.; Ruiz, I.; Ozkan, M.; Ozkan, C.S. Pillared graphene and silicon nanocomposite architecture for anodes of lithium ion batteries. In Proceedings of the SPIE NanoScience+ Engineering, San Diego, CA, USA; 2014.
25. Wang, W.; Ruiz, I.; Guo, S.; Favors, Z.; Bay, H.H.; Ozkan, M.; Ozkan, C.S. Hybrid carbon nanotube and graphene nanostructures for lithium ion battery anodes. *Nano Energy* **2014**, *3*, 113–118. [CrossRef]
26. Luo, J.; Liu, J.; Zeng, Z.; Ng, C.F.; Ma, L.; Zhang, H.; Lin, J.; Shen, Z.; Fan, H.J. Three-dimensional graphene foam supported Fe3O4 lithium battery anodes with long cycle life and high rate capability. *Nano Lett.* **2013**, *13*, 6136–6143. [CrossRef]
27. Yoo, E.; Kim, J.; Hosono, E.; Zhou, H.-s.; Kudo, T.; Honma, I. Large reversible Li storage of graphene nanosheet families for use in rechargeable lithium ion batteries. *Nano Lett.* **2008**, *8*, 2277–2282. [CrossRef]
28. Chen, S.; Chen, P.; Wang, Y. Carbon nanotubes grown in situ on graphene nanosheets as superior anodes for Li-ion batteries. *Nanoscale* **2011**, *3*, 4323–4329. [CrossRef]
29. Zhu, Y.; Li, L.; Zhang, C.; Casillas, G.; Sun, Z.; Yan, Z.; Ruan, G.; Peng, Z.; Raji, A.-R.O.; Kittrell, C. A seamless three-dimensional carbon nanotube graphene hybrid material. *Nat. Commun.* **2012**, *3*, 1225. [CrossRef]

30. Yan, Z.; Ma, L.; Zhu, Y.; Lahiri, I.; Hahm, M.G.; Liu, Z.; Yang, S.; Xiang, C.; Lu, W.; Peng, Z. Three-dimensional metal–graphene–nanotube multifunctional hybrid materials. *ACS Nano* **2012**, *7*, 58–64. [CrossRef]
31. Lin, C.; Wang, H.; Yang, W. The thermomutability of single-walled carbon nanotubes by constrained mechanical folding. *Nanotechnology* **2010**, *21*, 365708. [CrossRef]
32. Liu, J.; Yang, R. Tuning the thermal conductivity of polymers with mechanical strains. *Phys. Rev. B* **2010**, *81*, 174122. [CrossRef]
33. Xu, Z.; Buehler, M.J. Strain controlled thermomutability of single-walled carbon nanotubes. *Nanotechnology* **2009**, *20*, 185701. [CrossRef]
34. Lee, H.-F.; Kumar, S.; Haque, M. Role of mechanical strain on thermal conductivity of nanoscale aluminum films. *Acta Mater.* **2010**, *58*, 6619–6627. [CrossRef]
35. Wei, N.; Xu, L.; Wang, H.-Q.; Zheng, J.-C. Strain engineering of thermal conductivity in graphene sheets and nanoribbons: A demonstration of magic flexibility. *Nanotechnology* **2011**, *22*, 105705. [CrossRef] [PubMed]
36. Li, X.; Maute, K.; Dunn, M.L.; Yang, R. Strain effects on the thermal conductivity of nanostructures. *Phys. Rev. B* **2010**, *81*, 245318. [CrossRef]
37. Lee, J.; Varshney, V.; Brown, J.S.; Roy, A.K.; Farmer, B.L. Single mode phonon scattering at carbon nanotube-graphene junction in pillared graphene structure. *Appl. Phys. Lett.* **2012**, *100*, 183111–183114. [CrossRef]
38. Schelling, P.; Phillpot, S.; Keblinski, P. Phonon wave-packet dynamics at semiconductor interfaces by molecular-dynamics simulation. *Appl. Phys. Lett.* **2002**, *80*, 2484–2486. [CrossRef]
39. Wei, Z.; Chen, Y.; Dames, C. Wave packet simulations of phonon boundary scattering at graphene edges. *J. Appl. Phys.* **2012**, *112*, 024328. [CrossRef]
40. Lee, J.; Varshney, V.; Roy, A.K.; Farmer, B.L. Single mode phonon energy transmission in functionalized carbon nanotubes. *J. Chem. Phys.* **2011**, *135*, 104109. [CrossRef]
41. Park, J.; Lee, J.; Prakash, V. Phonon scattering at SWCNT–SWCNT junctions in branched carbon nanotube networks. *J. Nanoparticle Res.* **2015**, *17*, 1–13. [CrossRef]
42. Park, J.; Prakash, V. Phonon scattering and thermal conductivity of pillared graphene structures with carbon nanotube-graphene intramolecular junctions. *J. Appl. Phys.* **2014**, *116*, 014303. [CrossRef]
43. Muller-Plathe, F. A simple nonequilibrium molecular dynamics method for calculating the thermal conductivity. *J. Chem. Phys.* **1997**, *106*, 6082–6085. [CrossRef]
44. Resnick, A.; Mitchell, K.; Park, J.; Farfán, E.B.; Yee, T. Thermal transport study in actinide oxides with point defects. *Nucl. Eng. Technol.* **2019**, *51*, 1398–1405. [CrossRef]
45. Park, J.; Farfán, E.B.; Mitchell, K.; Resnick, A.; Enriquez, C.; Yee, T. Sensitivity of thermal transport in thorium dioxide to defects. *J. Nucl. Mater.* **2018**, *504*, 198–205. [CrossRef]
46. Park, J.; Bifano, M.F.; Prakash, V. Sensitivity of thermal conductivity of carbon nanotubes to defect concentrations and heat-treatment. *J. Appl. Phys.* **2013**, *113*, 034312. [CrossRef]
47. Mitchell, K.; Park, J.; Resnick, A.; Horner, H.; Farfan, E.B. Phonon scattering and thermal conductivity of actinide oxides with defects. *Appl. Sci.* **2020**, *10*, 1860. [CrossRef]
48. Park, J.; Farfán, E.B.; Enriquez, C. Thermal transport in thorium dioxide. *Nucl. Eng. Technol.* **2018**, *50*, 731–737. [CrossRef]
49. Park, J.; Pena, P.; Tekes, A. Thermal Transport Behavior of Carbon Nanotube–Graphene Junction under Deformation. *Int. J. Nanosci.* **2020**, *19*, 1950013. [CrossRef]
50. Plimpton, S. Fast parallel algorithms for short-range molecular dynamics. *J. Comput. Phys.* **1995**, *117*, 1–19. [CrossRef]
51. Sun, H. COMPASS: An ab initio force-field optimized for condensed-phase applications overview with details on alkane and benzene compounds. *J. Phys. Chem. B* **1998**, *102*, 7338–7364. [CrossRef]
52. Sun, H.; Ren, P.; Fried, J. The COMPASS force field: Parameterization and validation for phosphazenes. *Comput. Theor. Polym. Sci.* **1998**, *8*, 229–246. [CrossRef]
53. Sun, H.; Mumby, S.J.; Maple, J.R.; Hagler, A.T. An ab initio CFF93 all-atom force field for polycarbonates. *J. Am. Chem. Soc.* **1994**, *116*, 2978–2987. [CrossRef]
54. Hu, M.; Keblinski, P.; Schelling, P.K. Kapitza conductance of silicon–amorphous polyethylene interfaces by molecular dynamics simulations. *Phys. Rev. B* **2009**, *79*, 104305. [CrossRef]
55. Prasad, M.V.; Bhattacharya, B. Phonon wave-packet scattering and energy dissipation dynamics in carbon nanotube oscillators. *J. Appl. Phys.* **2015**, *118*, 244906. [CrossRef]
56. Wang, J.; Wang, J.-S. Single-mode phonon transmission in symmetry-broken carbon nanotubes: Role of phonon symmetries. *J. Appl. Phys.* **2009**, *105*, 063509. [CrossRef]
57. Stuart, S.J.; Tutein, A.B.; Harrison, J.A. A reactive potential for hydrocarbons with intermolecular interactions. *J. Chem. Phys.* **2000**, *112*, 6472. [CrossRef]
58. Grujicic, M.; Cao, G.; Gersten, B. Atomic-scale computations of the lattice contribution to thermal conductivity of single-walled carbon nanotubes. *Mater. Sci. Eng. B* **2004**, *107*, 204–216. [CrossRef]

59. Si, C.; Wang, X.-D.; Fan, Z.; Feng, Z.-H.; Cao, B.-Y. Impacts of potential models on calculating the thermal conductivity of graphene using non-equilibrium molecular dynamics simulations. *Int. J. Heat Mass Transf.* **2017**, *107*, 450–460. [CrossRef]
60. Zhang, X.; Chen, Z.; Chen, H.; Xu, L. Comparative studies of thermal conductivity for bilayer graphene with different potential functions in molecular dynamic simulations. *Results Phys.* **2021**, *22*, 103894. [CrossRef]